Biomedical Signal Processing and Control 6 (2011) 432–437

Contents lists available at ScienceDirect

Biomedical Signal Processing and Control

journal homepage: www.elsevier.com/locate/bspc

Short communication

Image despeckling using a non-parametric statistical model of wavelet coefficients

Jing Tian*, Li Chen

School of Computer Science and Technology, Wuhan University of Science and Technology, 430081, PR China

ARTICLE INFO

Article history:
Received 21 August 2010
Received in revised form 4 October 2010
Accepted 16 November 2010
Available online 24 December 2010

PACS:
42.30.Va
42.30.Wb

Keywords:
Image despeckling
Wavelet
Statistical model

ABSTRACT

This paper investigates the image despeckling issue in the wavelet domain. A *maximum a posteriori* (MAP) estimation-based image despeckling approach is proposed by incorporating a *non-parametric* statistical model into a Bayesian inference framework. The proposed non-parametric model formulates the marginal distribution of wavelet coefficients. It differs from conventional parametric models in that the proposed model is automatically adapted to the observed image data, rather than imposing an assumption about the distribution of the data. Experiments are conducted to demonstrate the superior performance of the proposed approach.

1. Introduction

Removing speckle noise plays a key role in medical image processing (e.g., medical ultrasonography), since the speckle noise significantly degrades the image quality and complicates diagnostic decisions for discriminating fine details in images [1,2]. Despite early developed spatial filters [3,4], wavelet-based technique has been considered a popular approach to remove the speckle noise. One common idea is to perform a logarithmic transformation to convert the multiplicative speckle noise into an additive noise [5,6], followed by a wavelet decomposition on the input noisy image to pack the energy of the image into a few large coefficients, then modify the noisy wavelet coefficients using certain shrinkage functions. Finally, the denoised image is reconstructed by performing an inverse wavelet transform, followed by an exponential transformation. There exists another category of despeckling approach that exploits the Taylor expansion of wavelet coefficients [7], instead of the exponential transformation. This paper is focused on the methods using the exponential transformation.

The key challenge of the above-mentioned wavelet-based despeckling technique is the development of the shrinkage function, which is usually obtained by employing a Bayesian estimator that uses a suitable *probability density function* (pdf) as a prior for modelling the wavelet coefficients of the image [7–12]. To achieve that, several statistical models have been developed in the literature, which include Laplacian model [13], generalized Gaussian model [14], Student-*t* model [15]. However, the performance of the above-mentioned parametric model-based approaches greatly depends on the effectiveness of the prior pdf for modelling the wavelet coefficients.

To tackle the above challenge, a *non-parametric* statistical model is proposed in this paper to formulate the marginal distribution of wavelet coefficients. Furthermore, a *maximum a posteriori* (MAP) estimation-based image denoising approach is derived by incorporating the proposed model into a Bayesian inference framework.

The rest of this paper is organized as follows. A problem formulation for removing speckle noise from images is provided in Section 2. Then the proposed image despeckling approach is presented in Section 3. Experimental results are provided in Section 4 to compare the performance of the proposed non-parametric model with conventional statistical models, and compare the proposed approach with a number of image despeckling approaches developed in the literature. Finally, Section 5 concludes this paper.

2. Problem formulation

A noisy image in spatial domain can be mathematically formulated as

$$g_i = f_i \epsilon_i, \tag{1}$$

* Corresponding author.
E-mail addresses: eejtian@gmail.com (J. Tian), chenli@ieee.org (L. Chen).

1746-8094/$ – see front matter © 2010 Elsevier Ltd. All rights reserved.
doi:10.1016/j.bspc.2010.11.006

where i represents the pixel index, g_i is the noisy pixel, f_i is the noise-free pixel and ϵ_i represents the speckle noise [7,8]. The multiplicative noise in (1) can be converted to an additive one by applying the log-transformation on both sides of (1) to arrive at

$$g_i^l = f_i^l + \epsilon_i^l, \tag{2}$$

where g_i^l, f_i^l and ϵ_i^l are log-transformed versions of g_i, f_i and ϵ_i, respectively. It has been justified in the literature that the distribution of the log-transformed speckle is close to a Gaussian distribution [5,6]. Furthermore, since the discrete wavelet transform is a linear operation, the wavelet coefficients of the log-transformed image corrupted by the speckle noise can be expressed as

$$y_i = x_i + n_i, \tag{3}$$

where y_i, x_i and n_i represent wavelet coefficients of g_i^l, f_i^l and ϵ_i^l, respectively. The mathematical relation between image's intensity information and their wavelet coefficients can be found in [8,9]. Based on the above formulations, the goal of image denoising is to recover each noise-free coefficient x_i based on its noisy counterpart y_i.

3. Proposed image despeckling approach

The aim of the proposed approach is to recover the noise-free wavelet coefficient x_i via its MAP estimator (denoted as $\hat{x}_i$) based on the noisy coefficient y_i as

$$\hat{x}_i = arg\max p(x_i|y_i). \tag{4}$$

According to the Bayes rule, (4) can be rewritten as

$$p(x_i|y_i) \propto p(y_i|x_i)p(x_i). \tag{5}$$

The formulation of (5) boils down to the formulations of its two product terms $p(y_i\,|\,x_i)$ and $p(x_i)$, respectively.

Firstly, according to (3), the term $p(y_i\,|\,x_i)$ is formulated as

$$p(y_i|x_i) = \frac{1}{\sqrt{2\pi}\sigma_n} e^{-((y_i-x_i)^2/2\sigma_n^2)}. \tag{6}$$

Secondly, to formulate the term $p(x_i)$, a non-parametric statistical model [16] is exploited in this paper as follows. The pdf $p(x_i)$ is determined by the summation of a number of kernel functions, which are centered at each observed noisy coefficient in the neighborhood Ω_i at the position x_i. Furthermore, the above-mentioned kernel function is suggested to be a Gaussian function with a mean, which is the observed noisy coefficient (say, y_j), and a standard deviation h_j, which is the standard deviation of all homogeneous coefficients covered by a 5×5 square window Ω_i. To summarize, the pdf $p(x_i)$ is defined as

$$p(x_i) \propto \sum_{y_j\in\Omega_i} K_j(x_i - y_j), \tag{7}$$

in which the function $K(\cdot)$ is a Gaussian function with mean zero and variance h_j [16]; that is

$$K_j(x) = \frac{1}{\sqrt{2\pi}h_j} e^{-(x^2/2h_j^2)}, \tag{8}$$

Substituting (8) into (7), that is, the pdf $p(x_i)$ is

$$p(x_i) \propto \sum_{y_j\in\Omega_i} \frac{1}{\sqrt{2\pi}h_j} e^{-((x_i-y_j)^2/2h_j^2)}. \tag{9}$$

It is important to point out that the proposed non-parametric model (9) is fundamentally different from the conventional parametric models, since the proposed model automatically adapts to the observed image data (through parameters y_j and h_j in (9)).

Next, the proposed wavelet coefficients model (9) needs to be incorporated into the Bayesian inference framework (5) to derive the MAP estimator of the noise-free coefficient. Since the proposed model (9) consists of a number of components (i.e., kernel functions), we use each component of (9) as the prior model to calculate its corresponding MAP estimator of the noise-free coefficient, and then combine all MAP estimators to be the final estimator of the noise-free coefficient. More specifically, substituting (6) and one component (say j-th) of (9) into (5), we get

$$p(x_i|y_i) \propto \frac{1}{\sqrt{2\pi}\sigma_n} e^{-((y_i-x_i)^2/2\sigma_n^2)} \frac{1}{\sqrt{2\pi}h_j} e^{-((x_i-y_j)^2/2h_j^2)}. \tag{10}$$

By setting the derivative of (10) to be zero with respect to x_i, we can obtain the MAP estimator of the noise-free coefficient (denoted as $\hat{x}_i^j$) as

$$\hat{x}_i^j = \frac{\sigma_n^2 y_j + h_j^2 y_i}{\sigma_n^2 + h_j^2}. \tag{11}$$

Finally, the estimated noise-free coefficient can be obtained by averaging all MAP estimators, which are obtained by using each component of (9) as the prior image model, respectively; that means

$$\hat{x}_i = \frac{1}{|\Omega_i|}\sum_{y_j\in\Omega_i} \hat{x}_i^j = \frac{1}{|\Omega_i|}\sum_{y_j\in\Omega_i} \frac{\sigma_n^2 y_j + h_j^2 y_i}{\sigma_n^2 + h_j^2}, \tag{12}$$

where $|\Omega_i|$ represents the number of coefficients in the neighborhood Ω_i. Furthermore, the noise variance σ_n^2 is estimated via $\hat{\sigma}_n = \text{median}|y_i|/0.6745$ [17], where the coefficient y_i belongs to the highest HH subband. Note that the definitions of LL and HH subband can be found in [17].

One key challenge of the proposed approach is how to determine Ω_i in (9). For that, *only* considers the homogeneous neighboring coefficients, which belong to the same category with that of the central coefficient, is exploited. To determine the homogeneous local neighboring coefficients, a bi-class coefficient classification approach, which is developed in [18], is used in this paper. More specifically, for a coefficient under consideration, its neighboring coefficients Ω_i in (9) can be determined by imposing a square-shape window on this coefficient pixel position. However, not all coefficients covered by this square-shape window are used in (9). We first apply a bi-class coefficient classification, which is developed in [18], to classify the coefficients into two categories. Second, we only substitute the neighboring coefficients, which belong to same category with the coefficient under consideration, into (9).

A summary of the proposed image despeckling approach is provided as follows:

Step 1. Perform the log-transformation of the observed noisy image.
Step 2. Apply the wavelet transform on the log-transformed image.
Step 3. Estimate each noise-free coefficient through (12), excluding those of the LL subband.
Step 4. Perform the inverse wavelet transform, followed by an exponential transformation, to obtain the denoised image.

4. Experimental results

4.1. Justification of proposed non-parametric statistical model equation kde full (9)

The first experiment is to justify the proposed non-parametric statistical model (9) by comparing it with other four models: Gaussian model, Laplacian model [13], generalized Gaussian model [14],

Fig. 1. Three test images used in this paper: (a) *Lena*; (b) *Barbara*; (b) *MRI*.

Table 1
The *Kolmogorov–Smirnov* performance [19] comparison of various models for formulating the distribution of wavelet coefficients.

Test image	Subband	Gaussian model	Laplacian model [13]	Generalized Gaussian model [14]	Student-*t* model [15]	Proposed model (9)
	HL2	0.1924	0.0774	0.0317	0.1337	**0.0030**
Lena	LH2	0.1910	0.0988	0.0396	0.0732	**0.0060**
	HH2	0.1746	0.0677	0.0269	0.1321	**0.0109**
	HL2	0.1558	0.0633	0.0212	0.0822	**0.0099**
Barbara	LH2	0.1568	0.0815	0.0235	0.1143	**0.0031**
	HH2	0.1948	0.1117	0.0376	0.0869	**0.0039**
	HL2	0.2043	0.0948	**0.0384**	0.2202	0.0445
MRI	LH2	0.1923	0.0968	0.0449	0.2125	**0.0361**
	HH2	0.1806	0.0782	0.0233	0.1452	**0.0035**

Table 2
The *Kullback–Liebler* performance [19] comparison of various models for formulating the distribution of wavelet coefficients.

Test image	Subband	Gaussian model	Laplacian model [13]	Generalized Gaussian model [14]	Student-*t* model [15]	Proposed model (9)
	HL2	0.5406	0.1422	0.0266	0.1534	**0.0003**
Lena	LH2	0.5252	0.1629	0.0204	0.0789	**0.0013**
	HH2	0.4641	0.1110	0.0237	0.1714	**0.0010**
	HL2	0.3832	0.0869	0.0084	0.1031	**0.0008**
Barbara	LH2	0.3705	0.1133	0.0160	0.1603	**0.0008**
	HH2	0.5669	0.2163	0.0233	0.0762	**0.0006**
	HL2	0.6278	0.2011	0.0259	0.4523	**0.0242**
MRI	LH2	0.5647	0.2039	0.0388	0.4208	**0.0180**
	HH2	0.5274	0.1528	0.0180	0.2201	**0.0017**

Student-*t* model [15], using two statistical metrics. The smaller metrics values indicate better performance, and their definitions are presented as follows: *Kolmogorov–Smirnov* metric [19]

$$d_{ks} = \max_{w \in \mathbf{R}} |F_h(w) - F_e(w)|, \tag{13}$$

where $F_h(w)$ and $F_e(w)$ denote the *cumulative density function* (cdf) of the prior pdf and the empirical cdf, respectively. *Kullback–Liebler* metric [19]

$$d_{kl} = \sum_{w \in \mathbf{R}} p_h(w) \ln\left(\frac{p_h(w)}{p_e(w)}\right), \tag{14}$$

where $p_h(w)$ and $p_e(w)$ denote the prior and the empirical pdfs, respectively.

Three test images 512×512 *Lena*, 512×512 *Barbara* and 256×256 *MRI*, as shown in Fig. 1, are applied on a two-level decomposition using a Daubechies's wavelet with eight vanishing moments. Then, the distributions of the second-level detail subbands are fitted with the above-mentioned models, which are further compared with the histogram of the wavelet coefficients in the sense of the above-mentioned two statistical metrics. The comparison is presented in Tables 1 and 2 where the proposed model is more consistent to the histogram of the wavelet coefficients than other four conventional models, by providing the best objective statistical performance.

4.2. Despeckling performance comparison

Three test images 512×512 *Lena*, 512×512 *Barbara* and 256×256 *MRI*, as shown in Fig. 1, are used in this paper to serve as the ground truth and compared with denoised images for the objective performance comparison. The synthetically speckled images are generated by multiplying the noise-free ground truth image with a speckle noise simulated by passing a complex Gaussian random process through a 3×3 averaging filter, since a short-term correlation is sufficient to account for real speckle noise, and then taking the magnitude of the filtered output [20]. Furthermore, a number of noisy images with different levels of speckle noise are generated by changing the standard deviation σ_n of the complex Gaussian random process.

The proposed approach is compared with other five image despeckling approaches; they are: Donoho and Johnstone's approach [17], Kaur et al.'s approach [21], Chang et al.'s approach [14], Luisier et al.'s approach [22], Pizurica et al.'s approach [20], Zhou and Cheng's approach [23]. All of the above five algorithms are

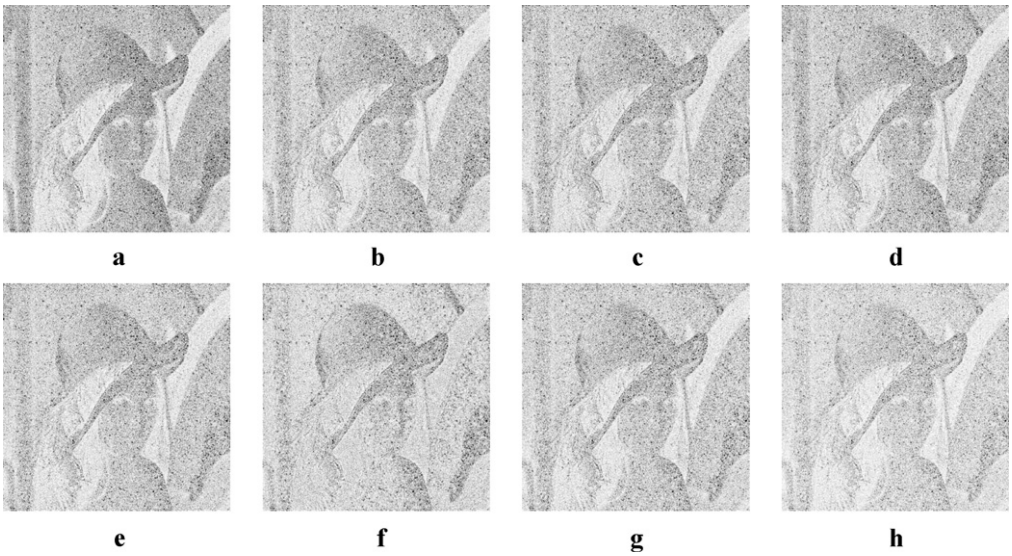

Fig. 2. The absolute difference images between the denoised images and the ground truth *Lena*, respectively. Furthermore, the intensity values of the absolute-differenced images are scaled up by four times for presentation, and the pixels with darker intensity indicate larger difference values yielded. (a) Noisy image ($\sigma_n = 0.2$); (b) Donoho and Johnstone's approach [17]; (c) Kaur et al.'s approach [21]; (d) Chang et al.'s approach [14]; (e) Luisier et al.'s approach [22]; (f) Pizurica et al.'s approach [20]; (g) Zhou and Cheng's approach [23]; and (h) the proposed approach.

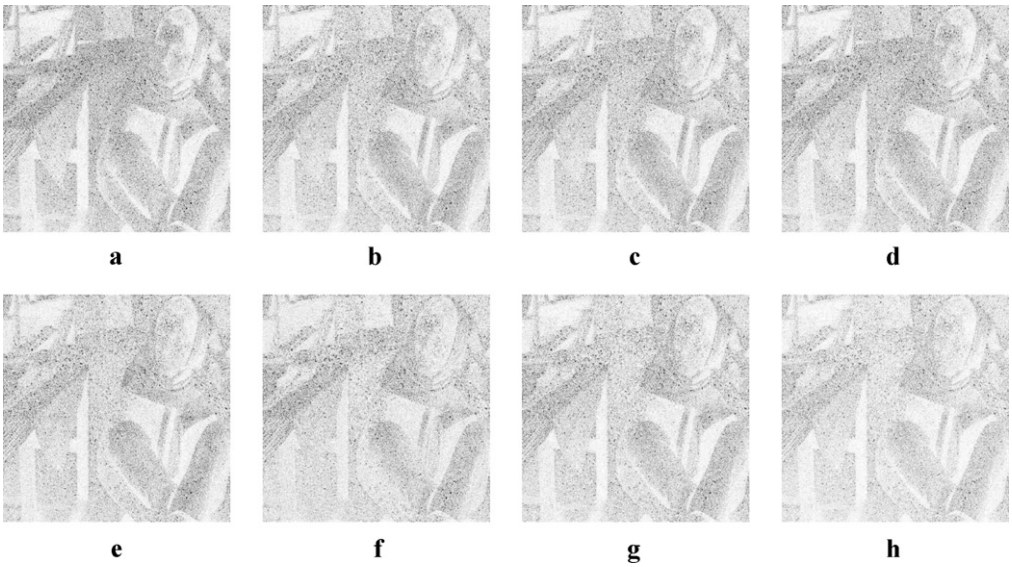

Fig. 3. The absolute difference images between the denoised images and the ground truth *Barbara*, respectively. Furthermore, the intensity values of the absolute-differenced images are scaled up by four times for presentation, and the pixels with darker intensity indicate larger difference values yielded. (a) Noisy image ($\sigma_n = 0.2$); (b) Donoho and Johnstone's approach [17]; (c) Kaur et al.'s approach [21]; (d) Chang et al.'s approach [14]; (e) Luisier et al.'s approach [22]; (f) Pizurica et al.'s approach [20]; (g) Zhou and Cheng's approach [23]; and (h) the proposed approach.

implemented using programs provided by their respective authors with suggested parameters setting. The wavelet decomposition is implemented via a five-level decomposition using a *Daubechies*'s wavelet with 8 vanishing moments.

Two image quality criteria are used in this paper to quantitatively measure the performance of various denoising approaches. The larger metrics values indicate better performance. Let $x_{i,j}$ and $\hat{x}_{i,j}$ denote the pixels at the position (i, j) of the original (i.e., the ground truth) image and the denoised image with a size of $M_1 \times M_2$ each, respectively. The first criterion is *peak signal noise ratio* (PSNR), which is defined as

$$\mathrm{PSNR} = 10 \times \log_{10} \frac{Q^2}{(1/M_1 \times M_2) \sum_{i=1}^{M_1} \sum_{j=1}^{M_2} (x_{i,j} - \hat{x}_{i,j})^2}, \tag{15}$$

where $Q = 255$ for 8-bit gray images. The second criterion is *edge-preservation index* (EPI) [7], which is defined as

$$\mathrm{EPI} = \frac{\sum(\Delta x - \overline{\Delta x}) \sum(\Delta \hat{x} - \overline{\Delta \hat{x}})}{\sqrt{\sum(\Delta x - \overline{\Delta x})^2 \sum(\Delta \hat{x} - \overline{\Delta \hat{x}})^2}}, \tag{16}$$

where Δx and $\Delta \hat{x}$ are high-pass filtered versions of original image x and denoised image $\hat{x}$ obtained with a 3×3 standard approximation of the Laplacian operator, respectively.

Tables 3 and 4 compare the PSNR and the EPI performances of the above mentioned methods, where the output values have been averaged over ten noise realizations. Figs. 2,3,4 provide the subjective performance comparison. As seen from the above tables and figures, the proposed algorithm always outperforms the above five

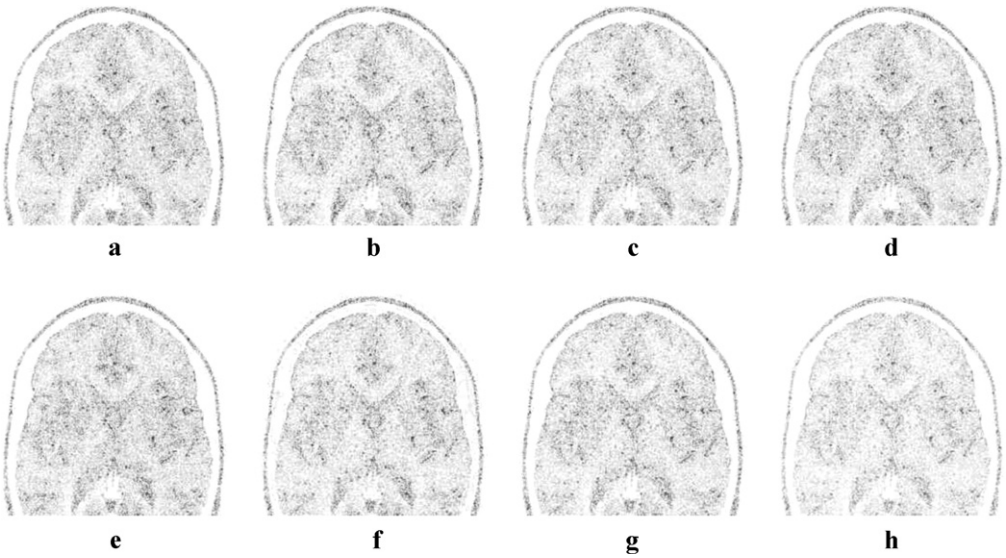

Fig. 4. The absolute difference images between the denoised images and the ground truth *MRI*, respectively. Furthermore, the intensity values of the absolute-differenced images are scaled up by four times for presentation, and the pixels with darker intensity indicate larger difference values yielded. (a) noisy image ($\sigma_n = 0.2$); (b) Donoho and Johnstone's approach [17]; (c) Kaur et al.'s approach [21]; (d) Chang et al.'s approach [14]; (e) Luisier et al.'s approach [22]; (f) Pizurica et al.'s approach [20]; (g) Zhou and Cheng's approach [23]; and (h) the proposed approach.

Table 3
The PSNR performance (15) comparison.

Algorithm	σ_n of simulated noise			Average
	0.2	0.4	0.6	
Test image Lena				
Ref. [17]	34.31	28.43	25.04	29.26
Ref. [21]	34.40	28.98	25.75	29.71
Ref. [14]	33.96	28.32	25.03	29.10
Ref. [22]	34.69	28.88	25.42	29.66
Ref. [20]	34.78	28.88	25.44	29.70
Ref. [23]	34.82	28.87	25.39	29.69
Proposed	34.85	28.94	25.46	29.75
Test image Barbara				
Ref. [17]	34.04	28.49	25.16	29.23
Ref. [21]	34.01	28.69	25.60	29.43
Ref. [14]	33.91	28.27	25.05	29.08
Ref. [22]	34.20	28.80	25.46	29.48
Ref. [20]	33.98	28.54	25.32	29.28
Ref. [23]	34.66	29.10	25.71	29.82
Proposed	34.73	29.09	25.69	29.84
Test image MRI				
Ref. [17]	36.10	31.01	27.91	31.67
Ref. [21]	36.39	30.78	27.71	31.63
Ref. [14]	36.28	30.56	27.39	31.41
Ref. [22]	35.83	31.08	28.09	31.67
Ref. [20]	34.53	30.24	27.31	30.69
Ref. [23]	36.46	31.27	28.27	32.00
Proposed	36.68	31.42	28.31	32.13

Table 4
The EPI [7] performance (16) comparison.

Algorithm	σ_n of simulated noise			Average
	0.2	0.4	0.6	
Test image Lena				
Ref. [17]	0.7986	0.5496	0.3979	0.5820
Ref. [21]	0.7965	0.5691	0.4187	0.5948
Ref. [14]	0.7894	0.5399	0.3928	0.5741
Ref. [22]	0.8059	0.5803	0.4216	0.6026
Ref. [20]	0.7931	0.5304	0.3672	0.5636
Ref. [23]	0.8328	0.5998	0.4358	0.6228
Proposed	0.8281	0.6016	0.4395	0.6231
Test image Barbara				
Ref. [17]	0.9638	0.8912	0.7922	0.8824
Ref. [21]	0.9632	0.8942	0.8055	0.8876
Ref. [14]	0.9648	0.8882	0.7900	0.8810
Ref. [22]	0.9625	0.9034	0.8145	0.8935
Ref. [20]	0.9673	0.8927	0.7931	0.8844
Ref. [23]	0.9713	0.9179	0.8370	0.9088
Proposed	0.9720	0.9187	0.8391	0.9099
Test image MRI				
Ref. [17]	0.9586	0.8816	0.7919	0.8774
Ref. [21]	0.9604	0.8754	0.7831	0.8730
Ref. [14]	0.9590	0.8681	0.7693	0.8654
Ref. [22]	0.9428	0.8799	0.7988	0.8739
Ref. [20]	0.9607	0.8755	0.7747	0.8703
Ref. [23]	0.9590	0.8902	0.8133	0.8875
Proposed	0.9634	0.8969	0.8149	0.8917

denoising methods to yield the best objective performance as well as the best subjective performance.

4.3. Computational Complexity

To explore the computational complexity, the above denoising approaches are implemented using the *Matlab* programming language and run on a PC with a Pentium 1.66 GHz CPU and a 2.99 GB RAM. Ten experiments are conducted for each of the above-mentioned approaches, then their average run times are compared in Table 5. As seen from Table 5, the computational load of the proposed approach is comparable to that of the conventional approaches.

Table 5
The run time (in seconds) comparison.

Algorithm	*Lena*	*Barbara*	*MRI*
Ref. [17]	1.61	1.78	0.55
Ref. [21]	1.73	1.56	0.53
Ref. [14]	1.61	1.52	0.53
Ref. [22]	2.06	2.09	0.49
Ref. [20]	7.70	7.11	1.60
Ref. [23]	9.86	9.50	2.53
Proposed approach	3.01	2.92	0.83

5. Conclusions

A new non-parametric Bayesian-based image despeckling approach has been proposed by incorporating a proposed non-

parametric statistical model for wavelet coefficients into a Bayesian framework and mathematically deriving a MAP estimation approach. The proposed statistical model outperforms the conventional models to formulate the distributions of wavelet coefficients. Furthermore, the proposed image despeckling approach is superior to the conventional image despeckling approaches, as verified in our experiments.

Acknowledgment

This work was supported by National Natural Science Foundation of China (Grant No. 60705012).

References

[1] J. Lee, L. Jurkevich, P. Dewaele, P. Wambacq, A. Oosterlinck, Speckle filtering of synthetic aperture radar images: a review, Remote Sens. Rev. 8 (1994) 313–340.
[2] R. Touzi, A review of speckle filtering in the context of estimation theory, IEEE Trans. Geosci. Remote Sens. 40 (2002) 2392–2404.
[3] Y. Yu, S.T. Acton, Speckle reducing anisotropic diffusion, IEEE Trans. Image Process. 11 (2002) 1260–1270.
[4] C. Loizou, C. Pattichis, C. Christodoulou, R. Istepanian, M. Pantziaris, A. Nicolaides, Comparative evaluation of despeckle filtering in ultrasound imaging of carotid artery, IEEE Trans. Ultrason. Ferroelectr. Freq. Control. 52 (2005) 1653–1669.
[5] H. Arsenault, G. April, Properties of speckle integrated with a finite aperture and logarithmically transformed, J. Opt. Soc. Am. 66 (1976) 1160–1163.
[6] H. Xie, L. Pierce, F. Ulaby, Statistical properties of logarithmically transformed speckle, IEEE Trans. Geosci. Remote Sens. 40 (2002) 721–727.
[7] S. Gupta, L. Kaur, R. Chauhan, S. Saxena, A versatile technique for visual enhancement of medical ultrasound images, Digital Signal Process. 17 (2007) 542–560.
[8] M. Bhuiyan, M. Ahmad, M. Swamy, Spatially adaptive thresholding in wavelet domain for despeckling of ultrasound images, IET Image Process. 3 (2009) 147–162.
[9] M. Bhuiyan, M. Ahmad, M. Swamy, Spatially adaptive wavelet-based method using the Cauchy prior for denoising the SAR images, IEEE Trans. Circ. Syst. Video Technol. 17 (2007) 500–507.
[10] G. Gao, Statistical modeling of sar images: a survey, Sensors 10 (2010) 775–795.
[11] L.N. Sharma, S. Dandapat, A. Mahanta, ECG signal denoising using higher order statistics in Wavelet subbands, Biomed. Signal Process. Control. 5 (2010) 214–222.
[12] J. Yan, Y. Lu, J. Liu, X. Wu, Y. Xu, Self-adaptive model-based ECG denoising using features extracted by mean shift algorithm, Biomed. Signal Process. Control. 5 (2010) 103–113.
[13] H. Rabbani, M. Vafadust, P. Abolmaesumi, S. Gazor, Speckle noise reduction of medical ultrasound images in complex wavelet domain using mixture priors, IEEE Trans. Biomed. Eng. 55 (2008) 2152–2160.
[14] S. Chang, B. Yu, M. Vetterli, Spatially adaptive wavelet thresholding with context modeling for image denoising, IEEE Trans. Image Process. 9 (2000) 1522–1531.
[15] I. Prudyus, S. Voloshynovskiy, A. Synyavskyy, Wavelet-based MAP image denoising using provably better class of stochastic i.i.d. image models, in: Proc. Int. Conf. on Telecommunications in Modern Satellite, Cable and Broadcasting Service, Nis, Yugoslavia, 2001, pp. 583–586.
[16] R. Duda, P. Hart, D. Stork, Pattern Classification, Wiley-Interscience, 2000.
[17] D. Donoho, I. Johnstone, Adapting to unknown smoothness via wavelet shrinkage, J. Am. Statist. Assoc. 90 (1995) 1200–1224.
[18] J. Tian, W. Yu, L. Ma, AntShrink: Ant colony optimization for image shrinkage, Pattern Recogn. Lett. 31 (2010) 1751–1758.
[19] L. Wasserman, All of Statistics, Springer, 2004.
[20] A. Pizurica, R. Pizurica, W. Philips, I. Lemahieu, M. Acheroy, A versatile wavelet domain noise filtration technique for medical imaging, IEEE Trans. Med. Imaging 22 (2003) 323–331.
[21] L. Kaur, S. Gupta, R. Chauhan, Image denoising using wavelet thresholding, in: Proc. Int. Conf. on Computer Vision, Graphics and Image Processing, Ahmadabad, India, 2002, pp. 1–6.
[22] F. Luisier, T. Blu, M. Unser, A new SURE approach to image denoising: interscale orthonormal wavelet thresholding, IEEE Trans. Image Process. 16 (2007) 593–606.
[23] D. Zhou, W. Cheng, Image denoising with an optimal threshold and neighbouring window, Pattern Recogn. Lett. 19 (2008) 1694–1697.